A study on the optimal spatial damping distribution in railway pantograph-catenary interaction

A study on the optimal spatial damping distribution in railway pantograph-catenary interaction

Dario Anastasio, Stefano Marchesiello, Luigi Garibaldi

Department of Mechanical and Aerospace Engineering, Politecnico di Torino, Corso Duca degli Abruzzi 24, 10129, Torino

https://doi.org/10.1080/00423114.2023.2200192

Cite as:

D. Anastasio, S. Marchesiello, L. Garibaldi, A study on the optimal spatial damping distribution in railway pantograph-catenary interaction, Vehicle System Dynamics, 2023, doi: 10.1080/00423114.2023.2200192.

A study on the optimal spatial damping distribution in railway pantograph-catenary interaction

Dario Anastasio*, Stefano Marchesiello, Luigi Garibaldi

Department of Mechanical and Aerospace Engineering, Politecnico di Torino, Corso Duca degli Abruzzi 24, 10129, Torino

**Corresponding author, email: dario.anastasio@polito.it*

Abstract

Railway overhead contact lines are very low-damped structures with a high modal density in the low-frequency region. This has a significant impact on the interaction with the pantograph, especially in the high-speed case and in multiple pantographs operations. This paper studies the optimal spatial damping distribution in overhead contact lines obtained by introducing localised damping connections, resulting in a non-proportional damping distribution. To this end, the simulation software Cateway is presented and adopted in conjunction with evolutionary multi-objective optimisers to seek for the most efficient spatial damping distribution. The study is conducted on a high-speed reference model considering two different train speeds. The final goal of this optimisation is to obtain useful hints about the most and least sensitive regions to damping modifications. A dedicated study on the locus of the poles of the system is also proposed to corroborate the findings of the analysis. Results show that significant improvements on the current collection quality can be achieved by carefully designing the spatial damping distribution, especially for the rear (trailing) pantograph. On the other hand, wrong design choices can lead to a degradation of the contact forces.

Keywords: pantograph-catenary; overhead contact line; non-proportional damping; contact force;

1. Introduction

The interaction between pantographs and the overhead contact line (OCL) is an important topic in railway transportation system that has been widely studied in the last decades, especially since the development of high-speed lines. The force exchanged between the pantographs and the OCL is called contact force and its statistical parameters are generally adopted as indicators of the current collection quality. National and interoperability regulations set rigid thresholds to the statistical values of the contact force to assure a smooth contact and to avoid undesired effects, such as electric arcs or losses of contact.

Given the difficulty of performing field measurements, several simulation software programs have been developed by the research community to study the dynamics of the pantograph-catenary interaction. This task is particularly challenging for multiple reasons: the complex geometrical arrangements of railway catenary systems, the computational cost and issues of simulating lines extending for kilometres, the rich dynamics of OCL structures and the intricate wave propagation phenomena they bring, the nonlinearities arising from contact and slackening phenomena. Bruni et al. proposed a benchmark study [1] comparing several methods for simulating the pantograph-catenary interaction, followed by a subsequent paper with new achievements [2]. More recently, Zhang et al. proposed a review of the pantograph-catenary interaction [3]. The usual way of modelling the overhead contact line is through finite element (FE) models [1,4–6], although methods based on Galerkin or modal superposition approaches have been developed as well [7–9]. As for the pantograph, the simplest model consists of a lumped-mass system having generally 3 degrees-of-freedom, but more refined multi-body models are adopted as well [2,10]. Several factors must be carefully analysed when performing such simulations, especially in the case of high-speed trains: problem initialisation (i.e. boundary conditions and static shape-finding) [11], model discretisation and numerical integration issues [7,12,13], the presence of nonlinear phenomena (mainly dropper slackening and loss of contact) [12]. Recent studies also analysed the influence of defects along the catenary [14], geometric irregularities [15,16], overlap sections [17,18], pantographs interval [19,20] and wind deflection [21].

Among all properties that influence the pantograph-catenary interaction, one crucial topic is related to damping. OCLs are known to be very low-damped structures with a high modal density in the low-frequency region [22–24]. This has a significant

impact on the interaction with the pantograph, as well as on the fatigue stress that is exerted on the OCL [7,13,25]. Therefore, being able to optimize the damping distribution of such structures might be an efficient way of improving the current collection quality of existing lines. This theoretically means gaining a smoother contact between the OCL and the pantograph(s), as well as the possibility to increase the train speed above the present limits, still in compliance with the current operational rules (for instance the TSI in Europe [26]). This is a particular issue in the case of two running pantographs, where the rear one (trailing) usually behave worse than the front one (leading). Several papers suggested that acting on the damping can be beneficial in terms of current collection quality [22,27–29], but a comprehensive study on the effects of a change in the damping distribution in the pantograph-catenary system has not been performed yet.

The present study aims to fill this gap by presenting a methodology to search for optimal damping in overhead contact lines. The idea is to intervene on the catenary by adding damping elements so as to alter its spatial damping distribution, and to seek for the effects of these changes in the current collection quality. To this end, the high-speed reference catenary of the standard EN50318 [30] is considered in this work. First, the simulation software called Cateway is presented [28] and its compliance with respect to the reference model of EN50318 is verified. This gives a valid reference for a standardised case, that can be used as a comparative measure when altering the damping distribution. The optimal damping distribution is then searched for by setting up an optimisation problem that aims to minimise the standard deviations of the leading and trailing contact forces. This process is performed using genetic algorithms [31] considering two different train speeds. A prior inspection is performed with a dedicated study on the locus of the poles of the system induced by the non-proportional spatial damping distribution [22].

The findings of this paper can give valid hints about the choice of installing damping elements in overhead contact lines and on their best position along the catenary length. Furthermore, the methodology here presented is very general and can be applied to overhead lines of potentially any railway infrastructure, giving a valid tool to exploit the potentialities of adding damping on existing or newly designed catenaries.

The paper is organised as follows: Section 2 introduces the simulation software and its compliance against the current standard. Section 3 introduces the optimisation problem and defines the variables to be optimised. Section 4 is devoted to preliminary

studies to set the limits of the optimisation, including the analysis on the locus of the system poles. Section 5 analyses and discusses the relevant findings of the optimisation. Eventually, conclusions are drawn in section 6.

2. Pantograph-catenary simulation software

Cateway is the pantograph-catenary dynamic software developed by the Dynamics and Identification Research Group of Politecnico di Torino. The software is based on Matlab programming language and it can be used to:

- simulate the pantograph-catenary interaction of AC and DC lines with multiple pantographs;
- simulate concentrated load tests, such impulse responses;
- perform the modal analysis of the OCL and the pantograph;
- evaluate the effects of variations in the simulation parameters, such as the tension of the wires;
- evaluate the effects of external disturbances or degradations of the contact wire;
- design new improvements for existing OCLs.

The main characteristics of the software are listed in the following paragraphs and its graphical interface can be seen in Figure 1.

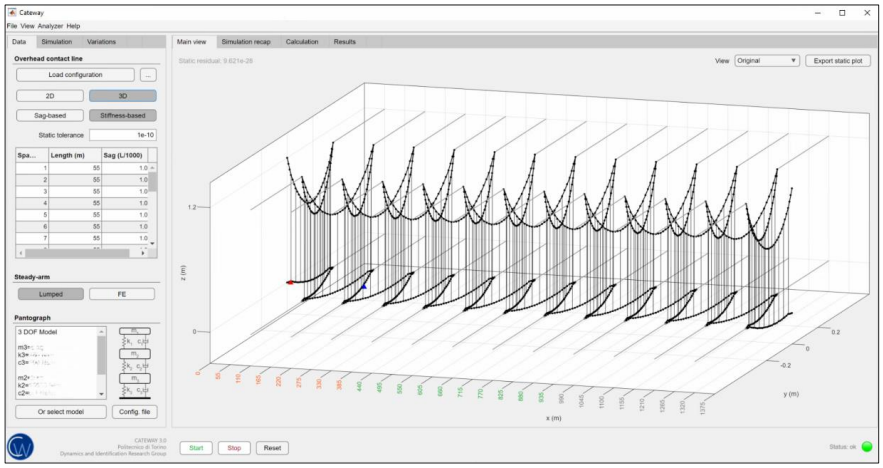

Figure 1: Graphical interface.

Catenary finite element model

The finite element model used for the catenary consists of 2D or 3D elements assembled according to the prescribed geometry. The software can handle several configurations, including multiple contact and messenger wires. Considering the simple case of Figure 2 for simplicity, the following elements are included in the model:

- Messenger and contact wires modelled as pre-tensioned Euler-Bernoulli beams with a user-selected spatial discretisation. The displacement of the first and last nodes of the considered catenary section is fixed in all the directions, so as to have a pinned boundary condition.
- Droppers modelled as bar elements with zero-stiffness in compression to account for the slackening phenomenon. The clamps are added as lumped masses to the corresponding nodes of the OCL.
- Steady-arms modelled as bar elements or as lumped elements with equivalent mass, axial stiffness and bending stiffness. In the first case, the bar element is linked to the contact wire on one end, and it has a hinge on the other end. The stagger is included in the 3D case.
- Brackets modelled as lumped stiffness and damping elements.

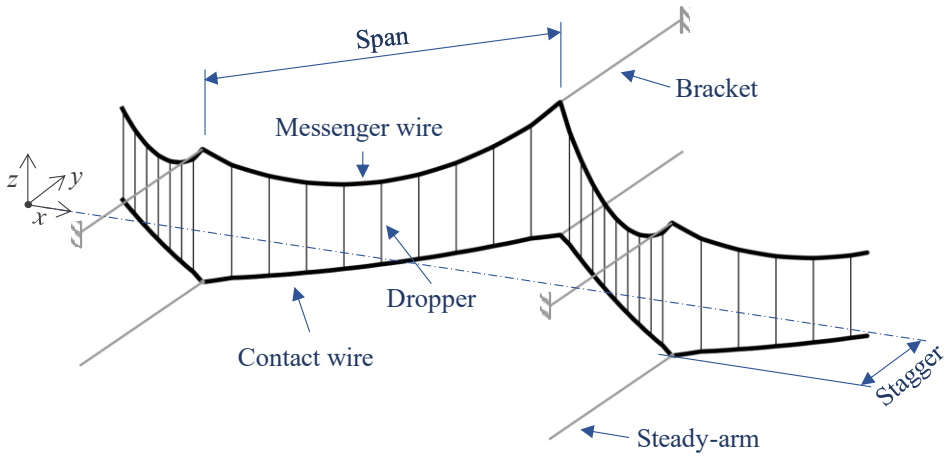

Figure 2: Simple railway catenary system.

The system matrices are assembled following the indications in [12]. After assembling the matrices, the equation of motion of the overhead contact line reads:

$$\mathbf{M}\ddot{\boldsymbol{\nu}} + \mathbf{C}\dot{\boldsymbol{\nu}} + \mathbf{K}\boldsymbol{\nu} = \mathbf{f}_{\mathrm{OCL}}, \tag{1}$$

where $\mathbf{M}$, $\mathbf{C}$ and $\mathbf{K}$ are the mass, damping and stiffness matrices of the overhead contact line, $\mathbf{f}_{\mathrm{OCL}}$ is the forcing vector and $\boldsymbol{\nu} = \left[\boldsymbol{\nu}_{\mathrm{MW}}^{\mathrm{T}} \ \boldsymbol{\nu}_{\mathrm{CW}}^{\mathrm{T}}\right]^{\mathrm{T}}$ is the vector of nodal deflections. This contains the nodal displacements on the three directions and the corresponding rotations. The subscripts $\cdot_{\mathrm{MW}}$ and $\cdot_{\mathrm{CW}}$ stand for “messenger wire” and “contact wire”.

Pantograph and contact models

The software can handle multiple pantographs operations with a user-selected distance. Each pantograph is modelled as a 3 degrees-of-freedom system with equivalent lumped parameters, as in [30]. An uplift force f_{up} is applied to the lowest DOF of the pantograph, while the contact force is computed with respect to the upper DOF, which slides along the contact wire with a constant speed v (Figure 3).

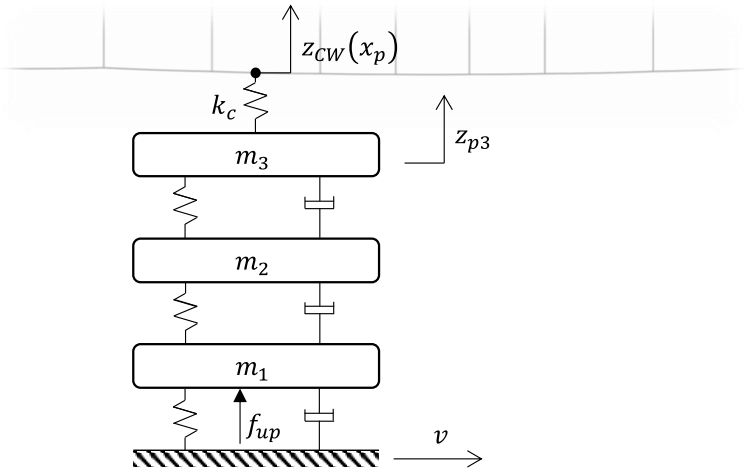

Figure 3: Pantograph and contact models.

The contact model is based on the penalty method, so that a contact stiffness k_c is defined. The contact force $f_c(t)$ is equal to

$$f_c(t) = \begin{cases} k_c\left(z_{p3}(t) - z_{CW}\left(x_p(t)\right)\right) & \text{if } z_{p3}(t) > z_{CW}\left(x_p(t)\right) \\ 0 & \text{elsewhere} \end{cases} \quad (2)$$

where $z_{p3}(t)$ is the displacement of the upper DOF of the pantograph model at time t and $z_{CW}\left(x_p(t)\right)$ is the displacement of the contact wire corresponding to the position x_p of the pantograph at time t, computed using classical Hermite shape functions of beam elements. The contact stiffness k_c is a crucial parameter in the penalty method, which derives from the Hertz theory of contact. In [32] it is reported that values of k_c between $1\ \mathrm{MN/m}$ and $4\ \mathrm{MN/m}$ are good and in the realistic range of Hertz theory for high-speed applications. Lower values act as a low-pass filter on the contact force, while higher values might lead to numerical issues. A value of $k_c = 2\ \mathrm{MN/m}$ is used in all the simulations presented in this paper. Note that the admissible values of k_c can be lowered if a contact damping parameter is added, as suggested in [33].

Problem initialisation and static shape-finding

Given the complex geometrical arrangements of the catenary, an iterative procedure is needed to obtain its static configuration. A static shape-finding problem must be set where the static equilibrium equations must be solved according to a target requirement set by the user. The software allows two paths: (*i*) the droppers lengths are set as a target; (*ii*) the contact wire pre-sag is set as a target. In the first case, the iteration is conducted by minimising the residual between the computed droppers lengths and the desired ones. Note that the length of the droppers is inversely proportional to their axial stiffness (in tension). The profile of the contact wire is therefore obtained a posteriori in this case. Conversely, in the second case the user defines the desired pre-sag of the contact wire, and the droppers lengths (and therefore stiffnesses) are obtained a posteriori. In both cases, the internal static forces acting on the droppers are obtained as an output. The calculation is iterative because of the relation between geometry and the exact tension in each wire [4,11]. The stiffness matrix is therefore updated at each iteration. As an example, two static configurations are depicted in Figure 4, obtained considering two catenaries from the reference model of EN50318 (AC-Simple and DC). The latter has two contact wires, depicted with two different colours.

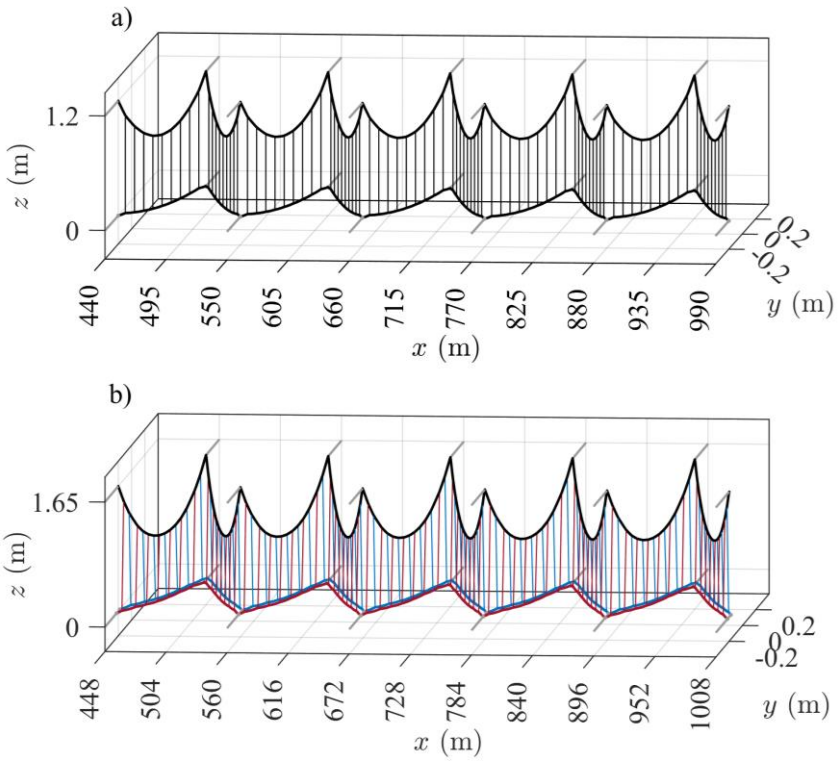

Figure 4: Static configurations of the overhead contact lines in EN50318. a) AC-Simple catenary; b) DC catenary.

Numerical integration

A dedicated study related to numerical issues arising from the travelling contact force at high-speed has been proposed in [7]. The choices of the numerical integrator and of the time and spatial discretisation steps are of critical importance when simulating the pantograph-catenary interaction. Generally speaking, a refined spatial mesh, a low time step and a robust implicit integration algorithm are key points to obtain a reliable simulation. Numerical damping can also be used to avoid spurious computational contributions, such as with the Generalized-α method [34]. The well-known Newmark method [35] is adopted in the following simulations of this work, with a time step of 0.5 ms and considering a spatial mesh of maximum 0.5 m. These values have been selected after a convergency analysis on the selected pantograph-catenary couple. The integration method has been modified to account for the loss of contact and droppers slackening nonlinearities, with iterations performed at each time step. The flowchart of the computational process is depicted in Figure 5.

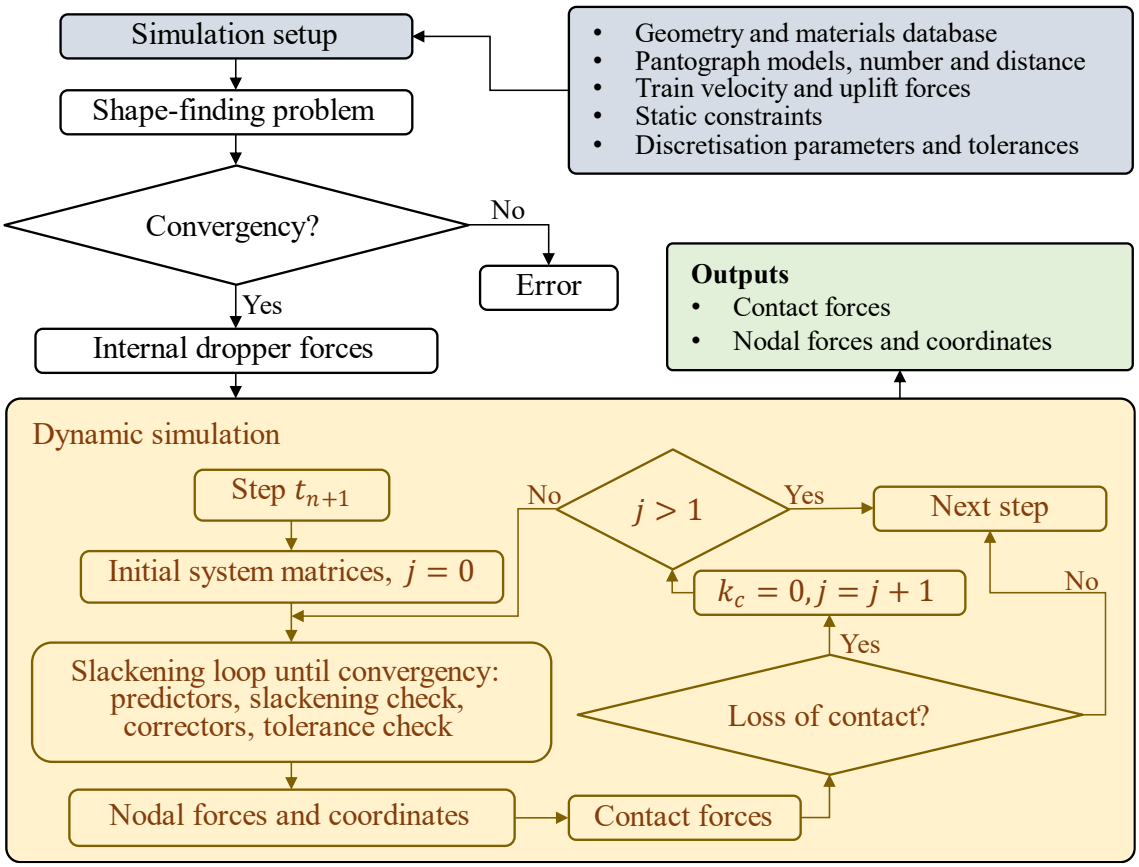

Figure 5: Flowchart of the computational process.

Compliance with the reference model AC-simple of EN50318

The standard EN50318 [30] defines some reference models to validate pantograph-catenary simulation tools. The AC-Simple model is used in this paper, corresponding to the high-speed catenary of Figure 4a with two pantographs and two velocities: 275 km/h and 320 km/h. The geometry consists of 25 equal spans of 55 m length. Damping is accounted for using a proportional damping model with given coefficients α and β for mass and stiffness matrices proportionality. The two pantographs are modelled as 3 degrees-of-freedom systems with the equivalent lumped parameters reported in the AC-Simple reference model of [30]. The 10 central spans in the range [385 – 935] m are used to compute the statistical values of the contact forces. The results are listed in Table 1 and confirm the compliance of the proposed software with respect to all the parameters of interest. The first row of each parameter corresponds to the leading (front) pantograph, while the second row is for the trailing (rear) pantograph.

Table 1: Comparison with the AC-Simple reference model of EN50318.

Parameter	**AC-Simple, 320 km/h**		**AC-Simple, 275 km/h**	
	Reference range	**Result**	**Reference range**	**Result**
Mean value (N)	[166.5-171.5] [166.5-171.5]	[170.1] [169.1]	[141.5-146.5] [141.5-146.5]	[142.5] [142.1]
Standard deviation 0-20 Hz (N)	[49.5-62.9] [30.2-43.8]	[50.6] [37.6]	[31.9-34.8] [50.0-54.5]	[33.5] [54.2]
Standard deviation 0-5 Hz (N)	[38.7-44.4] [14.3-23.3]	[40.2] [14.6]	[26.4-28.9] [41.2-45.4]	[26.7] [45.3]
Standard deviation 5-20 Hz (N)	[29.0-46.2] [26.7-38.2]	[30.7] [34.6]	[16.2-22.4] [25.2-34.7]	[20.2] [29.7]
Maximum value (N)	[295-343] [252-317]	[297] [282]	[219-244] [241-290]	[239] [289]
Minimum value (N)	[55-82] [21-86]	[67] [66]	[71-86] [14-50]	[78] [32]
Range of displacement (mm)	[39-51] [18-35]	[50] [26]	[38-49] [53-70]	[43] [58]
Maximum uplift (mm)	[57-64] [50-61]	[63] [57]	[39-48] [45-54]	[42] [45]
Loss of contact (%)	[0] [0]	[0] [0]	[0] [0]	[0] [0]

3. Optimal spatial damping distribution

The spatial distribution of damping in the overhead line is altered in this study to seek for the best distribution in terms of current collection quality. The final goal of this optimisation is to obtain useful hints about the most and least sensitive regions to damping

modifications. The study is conducted on the AC-Simple OCL described in Section 2 in order to have a valid reference for the standard case.

The cost function to be minimised is the standard deviation σ of the contact force in the frequency range 0-20 Hz. Since the reference model consists of two running pantographs, two standard deviations should be considered in the analysis. The subscripts $\cdot_l$ and $\cdot_t$ will refer to *leading* and *trailing* pantographs in the following and the standard deviations to be minimised are therefore called σ_l and σ_t. Calling $\sigma_{l,ref}$ and $\sigma_{t,ref}$ the reference values in the range 0-20 Hz, the percentage difference $\Delta\sigma_*$ can be defined as:

$$\Delta\sigma_* = 100\frac{\sigma_* - \sigma_{*,ref}}{\sigma_{*,ref}}, \quad *= l, t. \tag{3}$$

In order to keep the optimisation problem as general as possible, the two standard deviations are kept as two independent cost functions, so that the following multi-objective optimisation problem can be stated

$$\overline{\boldsymbol{\theta}} = \underset{\boldsymbol{\theta}\in\boldsymbol{\Theta}}{\operatorname{argmin}}(\sigma_l(\boldsymbol{\theta}), \sigma_t(\boldsymbol{\theta})), \tag{4}$$

where $\boldsymbol{\theta}$ is the vector of parameters to be optimised and $\boldsymbol{\Theta}$ is the feasible set of solution vectors.

A multi-objective genetic algorithm is adopted in this work to find the best set of parameters $\overline{\boldsymbol{\theta}}$. Genetic algorithms [31] belong to the class of evolutionary global optimisers, and they are commonly used to generate high-quality solutions to optimisation problems using biologically inspired mechanisms, such as reproduction, mutation and selection. Candidate solutions act like individuals in a population, which evolves through successive generations. A portion of the existing population is selected at each generation to breed a new offspring, and the selection is made upon the corresponding values of the cost function. Modifications can be introduced to better explore the range of possible solutions and avoid local minima. For instance, a mutation rate can be defined to introduce random changes to the existing solutions.

General settings and hypotheses

The damping distribution to be optimised is denoted as a function $\gamma(x)$ of the position x in the following. Since the analysed catenary is made of equal spans having the same length L, a periodicity constraint is added to reduce the size of the optimisation problem. This constraint imposes that the damping distribution function $\gamma(x)$ repeats itself equally on each span.

The easiest way to alter the damping distribution of the catenary is to add purely viscous damping connections between the contact wire and the messenger wire. Considering a single damping connection for each span, the function $\gamma(x)$ can be written as:

$$\gamma(x) = \begin{cases} c_l & \text{if } x = x_l \\ 0 & \text{elsewhere} \end{cases}, \tag{5}$$

where $0 \leq x_l \leq \mathrm{L}$ is the position of the lumped damping element and c_l is its value expressed in Ns/m.

4. Preliminary studies

The preliminary studies reported in this section aim to find the locations where an increase of the damping is most effective. To this end, two approaches are followed: first, the poles of the system are analysed when moving a single damping element along the span; second, the dynamic phenomena are considered by inspecting a full simulation with two running pantographs.

Study of the poles of the system with Ritz-Galerkin approach

The effect of a single damping connection to the poles of the system is inspected in this section. The evolution of the poles of the system if tracked by adding a single damping connection per span with $c_l = 50$ Ns/m and shifting its position along the span length.

The Ritz-Galerkin approach proposed in [7] is adopted to obtain the system matrices. These are then recast into a state-space formulation to perform the eigenvalue problem considering the non-proportional damping distribution. The Ritz-Galerkin method is adopted by considering only the vertical motion of the overhead contact line and by using a set of *N* comparison functions. These are given by the first *N* eigefunctions of a pinned-pinned Euler-Bernoulli beam of length $\mathrm{L_t} = \mathrm{L} \cdot n_{\mathrm{span}}$, with n_{span} equal to the total number of spans of the considered geometry:

$$\boldsymbol{\Phi} = \{\phi_n(x)\}_{N\times 1}, \qquad \phi_n = \sin\left(\frac{n\pi x}{\mathrm{L_t}}\right), \quad n = 1, \dots, N. \tag{6}$$

The mass and stiffness matrices $\mathbf{M}$, $\mathbf{K}$ are assembled as in [7] by summing the distributed and localised contributions and have dimensions $2N \times 2N$. The damping matrix $\mathbf{C}$ is instead written as the sum of the proportional damping part $\mathbf{C}_\mathrm{p}$ plus the non-

proportional one $\mathbf{C}_{\mathrm{np}}$. The latter is obtained by evaluating the lumped connections c_l at the positions $x_{l,d}$ of each span:

$$\begin{aligned} \mathbf{C} &= \mathbf{C}_{\mathrm{p}} + \mathbf{C}_{\mathrm{np}} = \alpha\mathbf{M} + \beta\mathbf{K} + c_l \begin{bmatrix} \boldsymbol{\Sigma}_D & -\boldsymbol{\Sigma}_D \\ -\boldsymbol{\Sigma}_D & \boldsymbol{\Sigma}_D \end{bmatrix}, \\ \boldsymbol{\Sigma}_D &= \sum_{d=1}^{D} \{\phi_n(x_{l,d})\}\{\phi_n(x_{l,d})\}^{\mathrm{T}}, \end{aligned} \tag{7}$$

where $D = n_{\mathrm{span}}$ is the total number of damping elements (one for each span), α and β are the proportional damping coefficients.

Introducing the state-space vector $\boldsymbol{\xi} = [\dot{\mathbf{z}}^{\mathrm{T}} \quad \mathbf{z}^{\mathrm{T}}]^{\mathrm{T}}$, the eigenvalue problem reads

$$\begin{aligned} (s\mathbf{A} + \mathbf{B})\boldsymbol{\xi} &= \mathbf{0}, \\ \mathbf{A} = \begin{bmatrix} \mathbf{C} & \mathbf{M} \\ \mathbf{M} & \boldsymbol{\mathcal{O}} \end{bmatrix}, \mathbf{B} &= \begin{bmatrix} \mathbf{K} & \boldsymbol{\mathcal{O}} \\ \boldsymbol{\mathcal{O}} & -\mathbf{M} \end{bmatrix}, \end{aligned} \tag{8}$$

with $\boldsymbol{\mathcal{O}}$ matrix of zeros of size $2N \times 2N$. The solution to Eq. (8) gives $2N$ pairs of complex-conjugate eigenvalues s_n with $n = 1, 2, \dots, 2N$. Given the non-proportional nature of the resulting damping distribution, it is possible to define $\Omega_n = |\Im[s_n]|$ as the modal frequency of the damped free vibration, and $\Gamma_n = -\Re[s_n]$ as the modal damping factor (see [36]).

It is known that the catenary modes come into groups, as a consequence of the low vertical stiffness of the steady-arms, and each group comprises a number of modes equal to the number of spans [7,13]. The geometry analysed in this paper consists of $n_{\mathrm{span}} = 25$ equal spans, therefore each group of modes contains 25 modes. The real and imaginary parts of the first 8 groups of poles are depicted in Figure 6 when shifting the position of the lumped damping connection. The number of comparison functions N is set to $N = 500$ in this analysis. It is observed how the imaginary parts $\Im[s_n]$ (associated with the modal damped frequencies Ω_n) remain almost constant, while the real parts $\Re[s_n]$ (associated with the modal damping factors Γ_n) show greater changes. For each span, the highest (negative) real parts are observed when x_l is lower than d_1 and higher than d_9, with a negative peak in correspondence of the support (L). Little changes are observed instead for all the other positions. This result suggests that the most effective region to add damping is around the support. For a better understanding of this behaviour, Figure 7 tracks the evolution of the first 8 groups of poles in the Argand-Gauss plane when increasing c_l from 0 to 100 Ns/m and fixing $x_l = \mathrm{L}$. It can be noted how the real parts of the poles increase up to 15 times with respect to the proportional damping

baseline. Interestingly, some of the poles start to come back towards lower real parts (see the magnified plot of Figure 7), similarly to what has been found in [22].

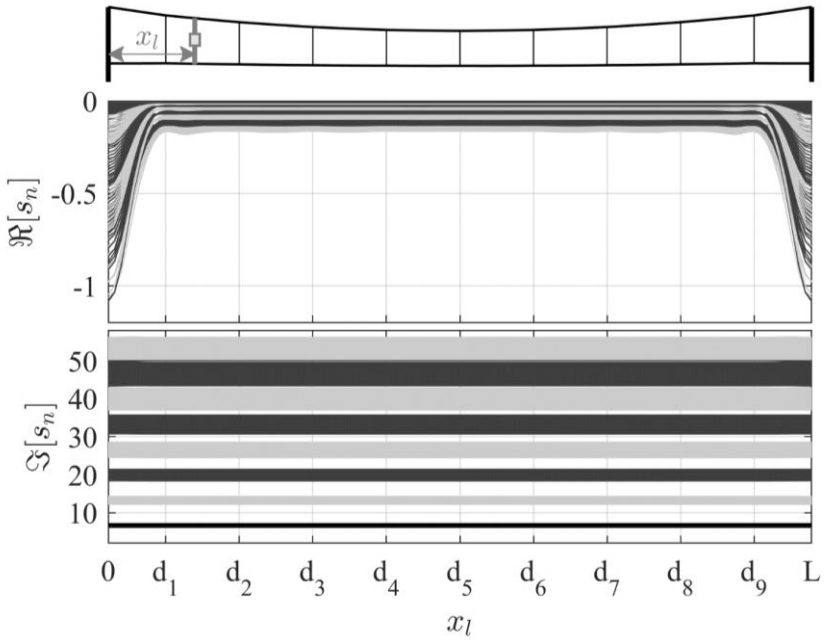

Figure 6: Real and imaginary parts of the poles of the system when shifting the damping connection. The value of c_l is 50 Ns/m. Odd groups of modes are depicted in dark grey and even groups in light grey.

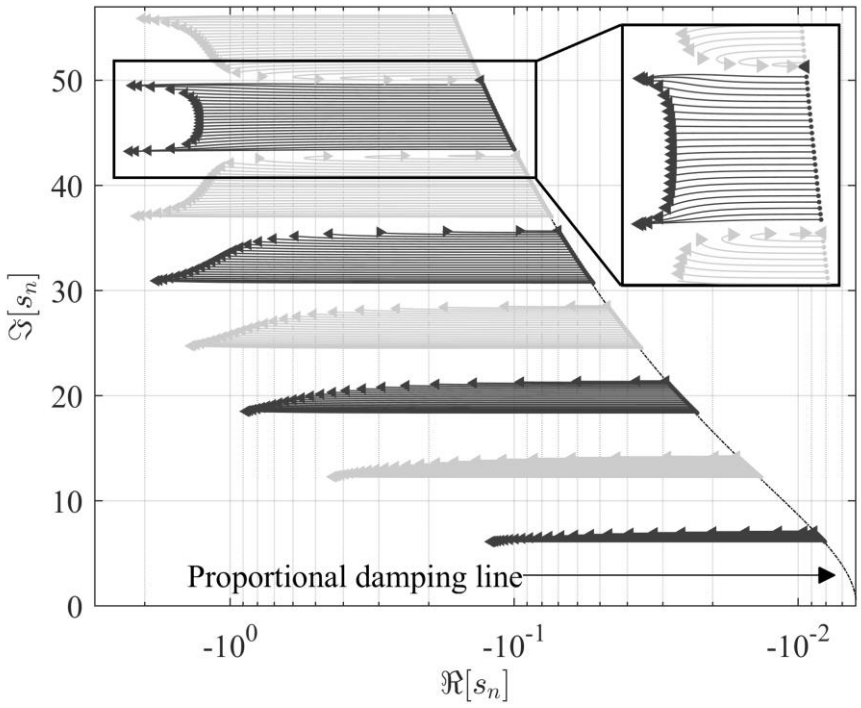

Figure 7: Locus of the poles of the system when increasing c_l from 0 to 100 Ns/m with x_l=L. Odd groups of modes are depicted in dark grey and even groups in light grey.

Dynamic simulation

The study of the system poles gives useful information, but does not consider dynamic effects such as vibrations induced by wave propagation phenomena and the interaction between multiple moving loads (pantographs). To account for these effects, a second analysis is carried out by inspecting the difference $\Delta\dot{z} = \dot{z}_{CW} - \dot{z}_{MW}$ between the vertical nodal velocities of the contact wire $\dot{z}_{CW}$ and the messenger wire $\dot{z}_{MW}$ in the full dynamic simulation with two running pantographs. The analysis is performed considering the reference case (without additional damping elements) with velocity v=320 km/h. The statistical parameters of the contact forces are therefore the ones listed in Table 1. A contour plot related to the quantity $\Delta\dot{z}$ s obtained in Figure 8 as the two pantographs pass by and the depicted span is the 10th, as illustrated in the y-axis.

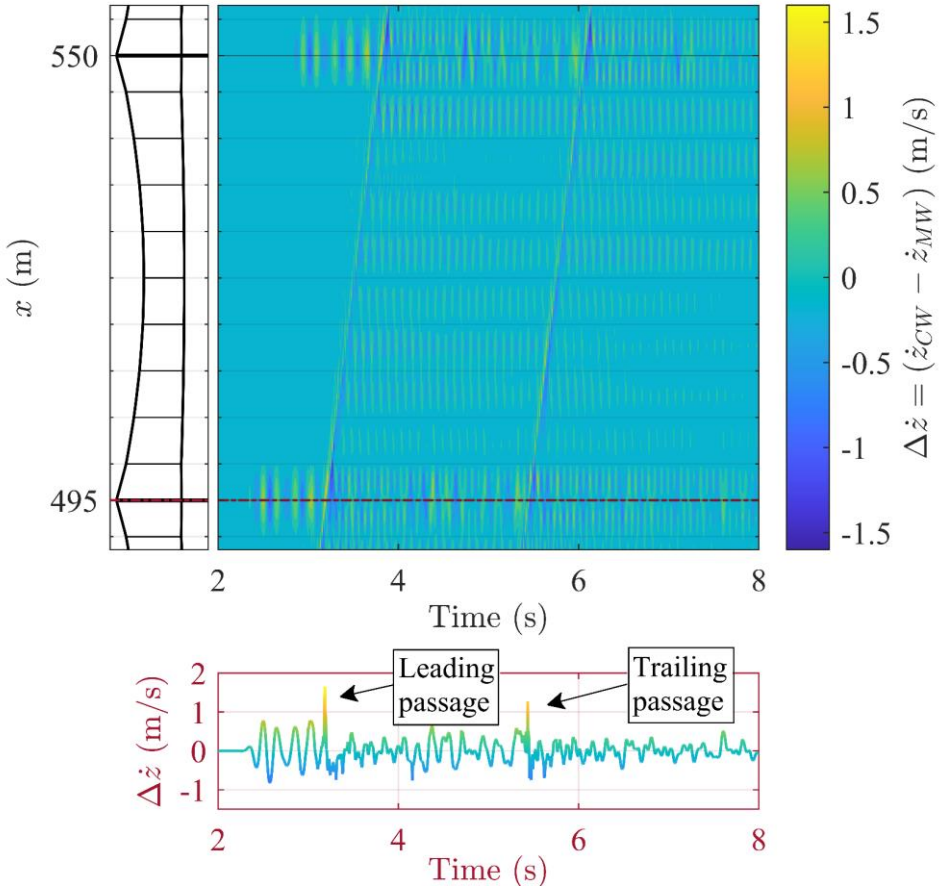

Figure 8: Contour plot of the velocity difference between contact and messenger wire for v=320 km/h. The dashed-dotted red line refers to the time history depicted in the red subplot.

Considering the magnitude of the velocity difference $|\Delta\dot{z}|$, its highest values are observed in the regions around the supports, i.e. between the last dropper of the previous span and the first dropper of the subsequent span, confirming the previous findings. A

detailed plot of the time history of $\Delta\dot{z}$ for the point $x = 495$ m (corresponding to a support) is also depicted. Furthermore, the relative velocities are almost zero in correspondence of the droppers, suggesting that adding damping to the existing droppers would not be an effective approach.

5. Optimisation results and discussion

In light of the outcomes of the previous section, the optimisation is carried out by adding a single lumped damper per span at a position x_l by inspecting the region around the supports. In particular, the range is limited to the 10 meters before and after. The values of c_l are analysed in the range 40-300 Ns/m with a discretisation of 20 Ns/m. The same catenary model of the previous sections (AC-Simple) is adopted and Cateway is used to produce all the results.

The values of the standard deviations of leading and trailing contact forces across the simulations are depicted in Figure 9 (a) and (b) for ν=275 km/h and ν=320 km/h, respectively. The solutions are plot together with the Pareto front [31], that represents the subset of most-efficient solutions. The reference values of Table 1 are indicated as dashed-dotted lines. Clearly, cases exist where a significant reduction in the standard deviations of the contact forces is possible. However, there are also combination of parameters resulting in a degradation of the standard deviations with respect to the reference case.

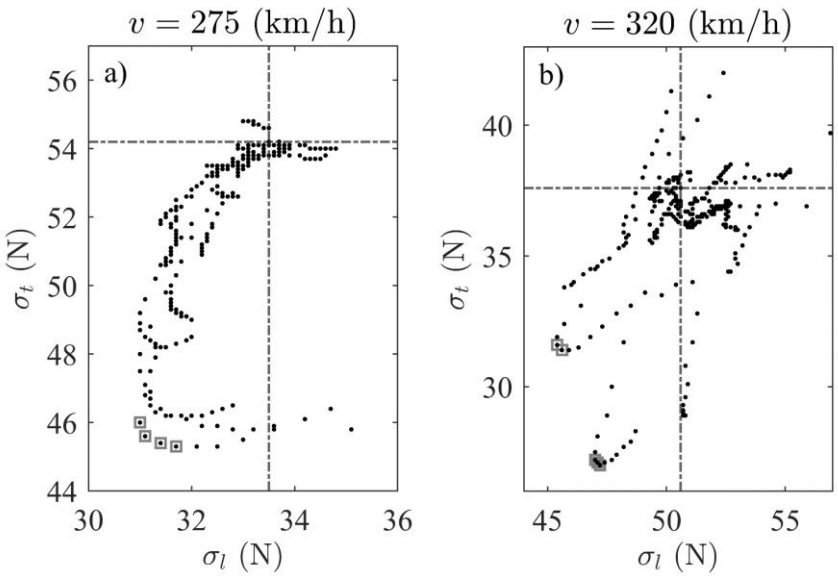

Figure 9: Optimisation results. Leading and trailing standard deviations across the simulations of the optimiser. The Pareto front is depicted with squares. Reference values (no added damping) are depicted with dashed-dotted lines. ν=275 km/h in (a) and ν=320 km/h in (b).

To better understand these results, Figure 10 shows the values of $\Delta\sigma_l$ and $\Delta\sigma_t$ in the form of contour plots with the x-axis representing the location x_l of the damping element and the y-axis representing the value c_l. The best combinations correspond to the areas tending towards a blue tint ($\Delta\sigma_* < 0$) , while the worst cases tend to a yellow tint ($\Delta\sigma_* > 0$). The highest reductions in the standard deviations of the contact forces are generally observed for the trailing pantograph and correspond to $\Delta\sigma_t = -16\%$ for v=275 km/h and $\Delta\sigma_t = -28\%$ for v=320 km/h. This result is not surprising, since the trailing pantograph generally resents of the oscillations induced by the passage of the leading pantograph. The addition of damping can attenuate this phenomenon, thus resulting in a smoother trailing contact force. Interestingly, the regions where $\Delta\sigma_t$ is minimum are different for the two velocities: the area of interest is centred around L for v=275 km/h, while it is located between L and d_1 for v=320 km/h. In both cases the best-performing values of c_l are between 100 Ns/m and 180 Ns/m.

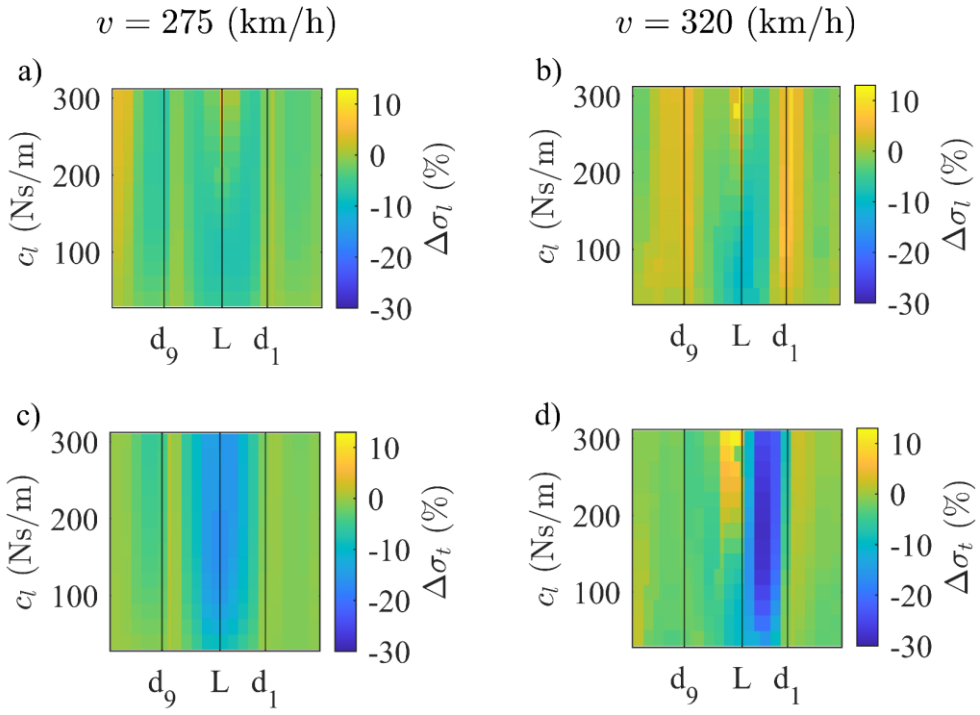

Figure 10: Optimisation results, contour plots of the variations of the standard deviations. $\Delta\sigma_l$ (leading) in (a),(b); $\Delta\sigma_t$ (trailing) in (b),(c). v=275 km/h in (a),(c) and v=320 km/h in (b),(d).

The parameters corresponding to the Pareto fronts are listed in Table 2 for the two velocities.

Table 2: Best parameters for the two velocities according to the Pareto front.

	x_l (m)	c_l (Ns/m)	$\Delta\sigma_l$ (%)	$\Delta\sigma_t$ (%)
v=275 km/h	55	100	-7.5	-15.1
	55	120	-7.2	-15.9
	55	140	-6.3	-16.2
	55	160	-5.4	-16.4
v=320 km/h	56	100	-10.3	-15.9
	56	120	-9.9	-16.5
	57	140	-7.1	-27.7
	57	160	-6.9	-27.9
	57	180	-6.7	-28.2

It is worth noting that Figure 10 shows also the areas where the inclusion of a damping connection degrades the contact forces. These areas are different for the two velocities and for leading and trailing contact forces, thus a generalisation is not possible. Optimisations like the one proposed in this paper must therefore be carried out for each overhead line geometry and for each working speed of interest, and considerations must be done on a case-by-case basis.

Taking the best and the worst solutions, the filtered contact forces in the range 0-20 Hz are depicted in Figure 11 for leading (a),(b) and trailing (c),(d) pantographs and for the two velocities as a function of the distance vt travelled by the pantograph. The reference solutions corresponding to the standardised case are also depicted as dashed black lines. As previously discussed, the benefits of the inclusion of damping elements are higher for the trailing pantograph, which generally shows lower maxima and higher minima with respect to the reference scenario.

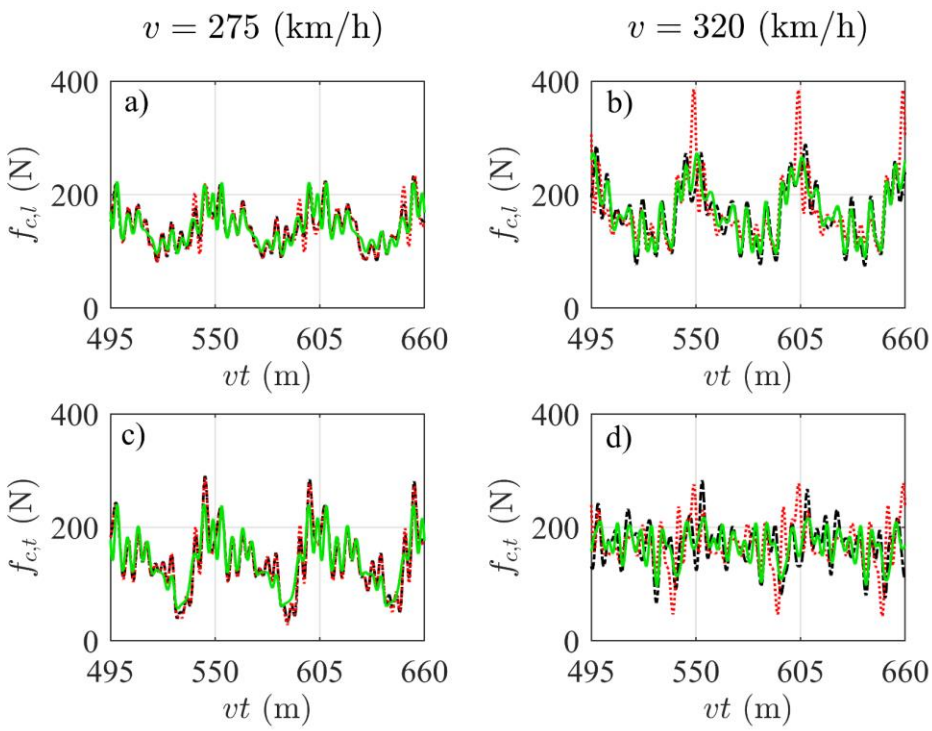

Figure 11: Optimisation results, filtered contact forces. Green lines: best solutions; dotted red lines: worst solutions; dashed black lines: reference solutions. Leading contact forces in (a), (b); trailing contact forces in (c),(d). v=275 km/h in (a),(c) and v=320 km/h in (b),(d).

The moving standard deviations of the contact forces are depicted in Figure 12 for the leading and the trailing pantographs as a function of the travelled distance vt. The window that is adopted is a sliding window with length equal to 55 m (one span). It can be seen how the best solutions (continue green lines) regularise the moving standard deviations towards lower values, especially when compared with the reference behaviour (dashed black lines).

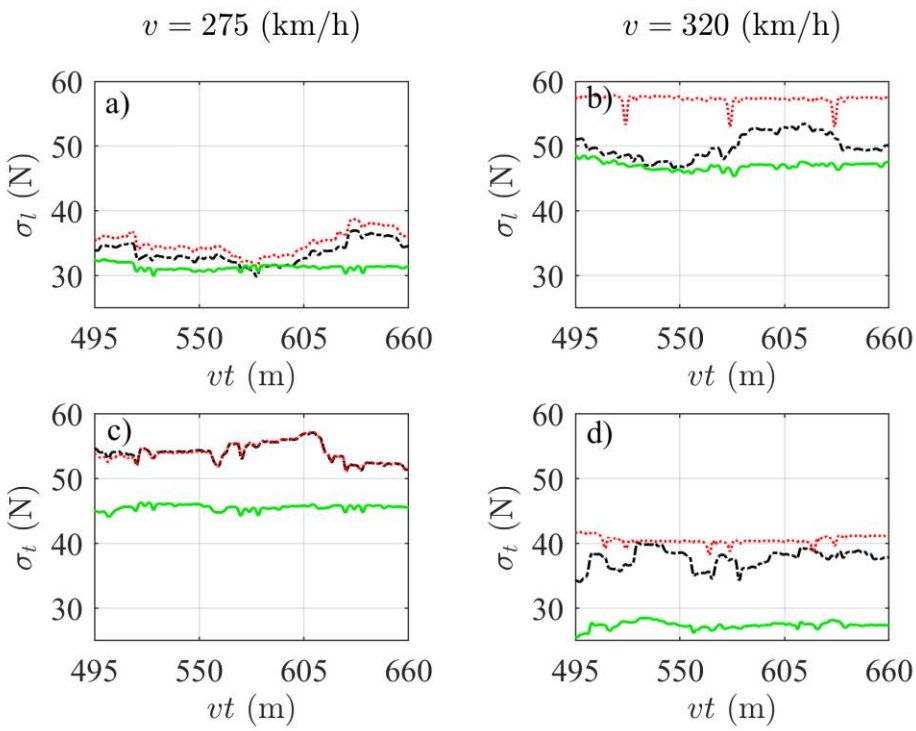

Figure 12: Optimisation results, standard deviations of the contact forces. Green lines: best solutions; dotted red lines: worst solutions; dashed black lines: reference solutions. Leading contact forces in (a), (b); trailing contact forces in (c),(d). v=275 km/h in (a),(c) and v=320 km/h in (b),(d).

Considerations about pantographs distance and speed

The optimisation presented in the previous section has been conducted considering the reference model (AC-Simple) with standardised parameters. In particular, the train speed v and the distance between the two pantographs d_p are the ones reported in the reference [30]. These parameters are known to be quite important in the current collection quality. The effect of adding damping elements is therefore investigated in this section considering two distance values $d_p = 100$ m and $d_p = 200$ m and 9 train speeds v in the range $[250\ 330]$ km/h. Simulations are first conducted without any damping element, and then repeated considering viscous damping connections with $x_l = 57$ m and $c_l = 160$ Ns/m. These values are selected by combining the results of the previous optimisations for 275 km/h and 320 km/h and taking the overall best parameters. For each velocity, the desired mean contact force value f_m is computed according to the prescription of the norm EN50367 [37] as $f_m = 0.00097v^2 + 70$ N, with v expressed in km/h.

The percentage differences $\Delta\sigma_l$ and $\Delta\sigma_t$ of Eq. (3) are considered again, taking as references the standard deviations without damping connections. Results are displayed in Figure 13a for $d_p = 100$ m and in Figure 13b for $d_p = 200$ m. The values of $\Delta\sigma_l$ and $\Delta\sigma_t$ are very different for the two pantographs distances, confirming the importance of this parameter in the contact force evaluation [19]. The added damping connection generally results in a reduction in the leading and trailing standard deviations inside the selected velocity range. It must be highlighted though that results are sensitive to the speed value, thus the extrapolation outside the analysed velocity range is not advisable without detailed analyses.

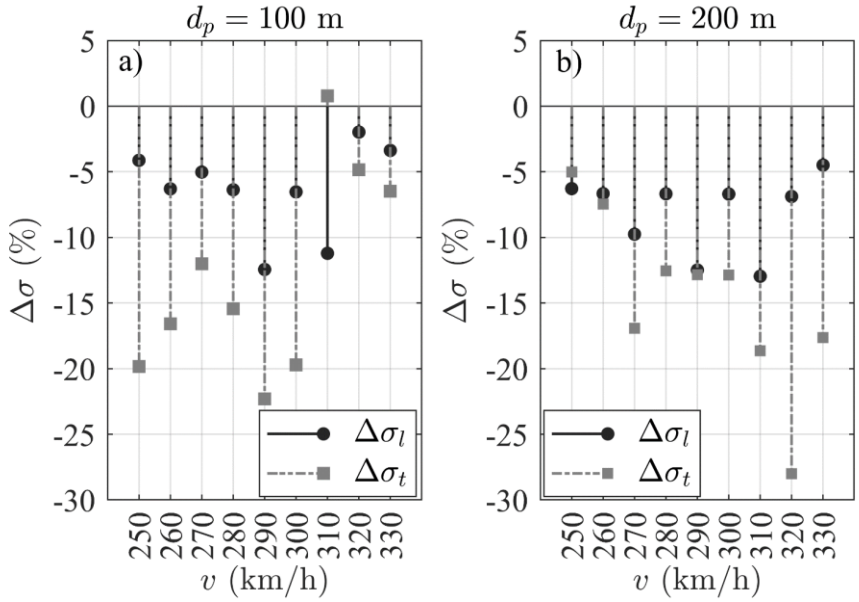

Figure 13: Variations of the standard deviations of leading (dots) and trailing (squares) contact forces for different train speeds and with x_l=57 m and c_l=160 Ns/m. a) Distance between the two pantographs equal to 100 m; b) Distance between the two pantographs equal to 200 m.

6. Conclusions

This paper presented a methodology to study the optimal spatial damping distribution in overhead contact lines obtained by introducing localised damping connections. The final goal of this optimisation was to obtain useful hints about the most and least sensitive regions to damping modifications with respect to the contact force exchanged between the contact wire and the pantograph. The simulation software Cateway has been presented and its main characteristics discussed. A reference model has been considered, consisting of a high-speed catenary with two running pantographs and two train speeds. The compliance of the software with respect to the reference case has been verified first

(standard EN50318, AC-Simple model). Cateway has then been used in conjunction with evolutionary multi-objective optimisers to seek for the most efficient spatial damping distribution. The results show that the spatial regions where damping connections are most effective are around the supports, and significant improvements in the current collection quality can be achieved especially for the rear (trailing) pantograph. However, combinations of parameters that lead to a degradation of the contact forces are possible as well. The influence of the pantographs distance and speed has been also discussed considering two distance values and nine train speed values. The results confirm that the quality of the current collection is quite sensitive to these parameters even in the case of added damping connections. A generalisation of the specific findings of this study is therefore not prudent, but the methodology here proposed can be extended to any pantograph-catenary couple to seek for the best spatial damping distribution on a case-by-case basis. Future work may include practical implementations and designs for the damping elements and the evaluation of their effects on overlap sections.

Statements and Declarations

The authors declare that no funds, grants, or other support were received during the preparation of this manuscript. The authors have no relevant financial or non-financial interests to disclose.

References

[1] S. Bruni, J. Ambrosio, A. Carnicero, Y.H. Cho, L. Finner, M. Ikeda, S.Y. Kwon, J.P. Massat, S. Stichel, M. Tur, W. Zhang, The results of the pantograph-catenary interaction benchmark, Vehicle System Dynamics. 53 (2015) 412–435. https://doi.org/10.1080/00423114.2014.953183.

[2] S. Bruni, G. Bucca, M. Carnevale, A. Collina, A. Facchinetti, Pantograph–catenary interaction: recent achievements and future research challenges, International Journal of Rail Transportation. 6 (2018) 57–82. https://doi.org/10.1080/23248378.2017.1400156.

[3] W. Zhang, D. Zou, M. Tan, N. Zhou, R. Li, G. Mei, Review of pantograph and catenary interaction, Front. Mech. Eng. 13 (2018) 311–322. https://doi.org/10.1007/s11465-018-0494-x.

[4] J.P. Massat, E. Balmes, J.P. Bianchi, G.V. Kalsbeek, OSCAR statement of methods, Vehicle System Dynamics. 53 (2015) 370–379. https://doi.org/10.1080/00423114.2015.1005016.

[5] J. Ambrósio, J. Pombo, P. Antunes, M. Pereira, PantoCat statement of method, 2015.

[6] P.A. Jönsson, S. Stichel, C. Nilsson, CaPaSIM statement of methods, Vehicle System Dynamics. 53 (2015) 341–346. https://doi.org/10.1080/00423114.2014.999799.

[7] S. Sorrentino, D. Anastasio, A. Fasana, S. Marchesiello, Distributed parameter and finite element models for wave propagation in railway contact lines, Journal of Sound and Vibration. 410 (2017) 1–18. https://doi.org/10.1016/j.jsv.2017.08.008.
[8] S. Gregori, M. Tur, E. Nadal, J.V. Aguado, F.J. Fuenmayor, F. Chinesta, Fast simulation of the pantograph–catenary dynamic interaction, Finite Elements in Analysis and Design. 129 (2017) 1–13. https://doi.org/10.1016/j.finel.2017.01.007.
[9] S. Gregori, M. Tur, A. Pedrosa, J.E. Tarancón, F.J. Fuenmayor, A modal coordinate catenary model for the real-time simulation of the pantograph-catenary dynamic interaction, Finite Elements in Analysis and Design. 162 (2019) 1–12. https://doi.org/10.1016/j.finel.2019.05.001.
[10] P. Ramalho, P. Antunes, J. Ambrósio, A.M. Macedo, S. Pissarra, Virtual pantograph-catenary environment for control development based on a co-simulation approach, Multibody Syst Dyn. 55 (2022) 241–265. https://doi.org/10.1007/s11044-022-09826-z.
[11] O. Lopez-Garcia, A. Carnicero, V. Torres, Computation of the initial equilibrium of railway overheads based on the catenary equation, Engineering Structures. 28 (2006) 1387–1394. https://doi.org/10.1016/j.engstruct.2006.01.007.
[12] Y.H. Cho, Numerical simulation of the dynamic responses of railway overhead contact lines to a moving pantograph, considering a nonlinear dropper, Journal of Sound and Vibration. 315 (2008) 433–454. https://doi.org/10.1016/j.jsv.2008.02.024.
[13] O. Vo Van, J.P. Massat, E. Balmes, Waves, modes and properties with a major impact on dynamic pantograph-catenary interaction, Journal of Sound and Vibration. 402 (2017) 51–69. https://doi.org/10.1016/j.jsv.2017.05.008.
[14] Y. Song, Z. Liu, X. Lu, Dynamic Performance of High-Speed Railway Overhead Contact Line Interacting with Pantograph Considering Local Dropper Defect, IEEE Transactions on Vehicular Technology. 69 (2020) 5958–5967. https://doi.org/10.1109/TVT.2020.2984060.
[15] Y. Song, P. Antunes, J. Pombo, Z. Liu, A methodology to study high-speed pantograph-catenary interaction with realistic contact wire irregularities, Mechanism and Machine Theory. 152 (2020). https://doi.org/10.1016/j.mechmachtheory.2020.103940.
[16] O. Vo Van, J.-P. Massat, C. Laurent, E. Balmes, Introduction of variability into pantograph–catenary dynamic simulations, Vehicle System Dynamics. 52 (2014) 1254–1269. https://doi.org/10.1080/00423114.2014.922199.
[17] S. Gregori, J. Gil, M. Tur, J.E. Tarancón, F.J. Fuenmayor, Analysis of the overlap section in a high-speed railway catenary by means of numerical simulations, Engineering Structures. 221 (2020). https://doi.org/10.1016/j.engstruct.2020.110963.
[18] Y. Song, A. Rønnquist, T. Jiang, P. Nåvik, Railway pantograph-catenary interaction performance in an overlap section: Modelling, validation and analysis, Journal of Sound and Vibration. 548 (2023). https://doi.org/10.1016/j.jsv.2022.117506.
[19] J. Pombo, P. Antunes, J. Ambrósio, A study on multiple pantograph operations for high-speed catenary contact, in: Civil-Comp Proceedings, Civil-Comp Press, 2012. https://doi.org/10.4203/ccp.99.139.
[20] Z. Xu, Y. Song, Z. Liu, Effective Measures to Improve Current Collection Quality for Double Pantographs and Catenary Based on Wave Propagation Analysis, IEEE Transactions on Vehicular Technology. 69 (2020) 6299–6309. https://doi.org/10.1109/TVT.2020.2985382.

[21] Y. Song, M. Zhang, O. Øiseth, A. Rønnquist, Wind deflection analysis of railway catenary under crosswind based on nonlinear finite element model and wind tunnel test, Mechanism and Machine Theory. 168 (2022) 104608. https://doi.org/10.1016/j.mechmachtheory.2021.104608.
[22] D. Anastasio, A. Fasana, L. Garibaldi, S. Marchesiello, Analytical investigation of railway overhead contact wire dynamics and comparison with experimental results, Mechanical Systems and Signal Processing. 116 (2019) 277–292. https://doi.org/10.1016/j.ymssp.2018.06.021.
[23] P. Nåvik, A. Rønnquist, S. Stichel, Identification of system damping in railway catenary wire systems from full-scale measurements, Engineering Structures. 113 (2016) 71–78. https://doi.org/10.1016/j.engstruct.2016.01.031.
[24] T. Jiang, A. Rønnquist, Y. Song, G.T. Frøseth, P. Nåvik, A detailed investigation of uplift and damping of a railway catenary span in traffic using a vision-based line-tracking system, Journal of Sound and Vibration. 527 (2022) 116875. https://doi.org/10.1016/j.jsv.2022.116875.
[25] J.P. Massat, T.M.L.N. Tajan, H. Maitournam, E. Balmes, Fatigue analysis of catenary contact wires for high speed trains, in: 9th World Congress on RailwayResearch, Lille, France, 2011: pp. 1–11.
[26] European Commission, COMMISSION REGULATION (EU) No.1299/2014 of 18 November 2014, on the technical specification for interoperability relating to the infrastructure subsystem of the rail system in the European Union, 2014.
[27] S. Harada, M. Shimizu, K. Ikeda, J. Sato, S. Koyano, K. Chikanari, Development of Simple Catenary Equipment Using PHC Contact Wire for Shinkansen, QR of RTRI. 49 (2008) 96–102. https://doi.org/10.2219/rtriqr.49.96.
[28] D. Anastasio, S. Marchesiello, L. Garibaldi, C. Spalvieri, A. Iacomelli, Improvements of the pantograph-catenary interaction: numerical simulations and experimental tests on the Italian high-speed overhead contact line, in: The Fifth International Conference on Railway Technology: Research, Development and Maintenance, Montpellier, France, 2022.
[29] M. Zhu, S.Y. Zhang, J.Z. Jiang, J. Macdonald, S. Neild, P. Antunes, J. Pombo, S. Cullingford, M. Askill, S. Fielder, Enhancing pantograph-catenary dynamic performance using an inertance-integrated damping system, Vehicle System Dynamics. 60 (2022) 1909–1932. https://doi.org/10.1080/00423114.2021.1884273.
[30] CENELEC, EN50318 - Railway applications - Current collection systems - Validation of simulation of the dynamic interaction between pantograph and overhead contact line, (2018).
[31] K. Deb, Multi-objective optimization using evolutionary algorithms, 1st ed, John Wiley & Sons, Chichester ; New York, 2001.
[32] O. Vo Van, Introduction of variability into pantograph-catenary dynamic simulations, Theses, Ecole nationale supérieure d'arts et métiers - ENSAM, 2016. https://pastel.archives-ouvertes.fr/tel-01404271.
[33] A. Collina, S. Bruni, Numerical simulation of pantograph-overhead equipment interaction, Vehicle System Dynamics. 38 (2002) 261–291. https://doi.org/10.1076/vesd.38.4.261.8286.
[34] J. Chung, G.M. Hulbert, A Time Integration Algorithm for Structural Dynamics With Improved Numerical Dissipation: The Generalized-α Method, Journal of Applied Mechanics. 60 (1993) 371–375. https://doi.org/10.1115/1.2900803.
[35] N.M. Newmark, A Method of Computation for Structural Dynamics, J. Engrg. Mech. Div. 85 (1959) 67–94. https://doi.org/10.1061/JMCEA3.0000098.

[36] S. Sorrentino, S. Marchesiello, B.A.D. Piombo, A new analytical technique for vibration analysis of non-proportionally damped beams, Journal of Sound and Vibration. 265 (2003) 765–782. https://doi.org/10.1016/S0022-460X(02)01560-2.
[37] CENELEC, EN50367 - Railway applications -Current collection systems - Technical criteria for the interaction between pantograph and overhead line, (2006).